

Packing Hyperspheres in High-Dimensional Euclidean Spaces

Monica Skoge,¹ Aleksandar Donev,^{2,3} Frank H. Stillinger,⁴ and Salvatore Torquato^{2,3,4,5,*}

¹Department of Physics, Princeton University, *Princeton, NJ 08544*

²Program in Applied and Computational Mathematics,
Princeton University, *Princeton NJ 08544*

³PRISM, Princeton University, *Princeton NJ 08544*

⁴Department of Chemistry, Princeton University, *Princeton NJ 08544*

⁵Princeton Center for Theoretical Physics,
Princeton University, *Princeton NJ 08544*

Abstract

We present the first study of disordered jammed hard-sphere packings in four-, five- and six-dimensional Euclidean spaces. Using a collision-driven packing generation algorithm, we obtain the first estimates for the packing fractions of the maximally random jammed (MRJ) states for space dimensions $d = 4, 5$ and 6 to be $\phi_{MRJ} \simeq 0.46, 0.31$ and 0.20 , respectively. To a good approximation, the MRJ density obeys the scaling form $\phi_{MRJ} = c_1/2^d + (c_2 d)/2^d$, where $c_1 = -2.72$ and $c_2 = 2.56$, which appears to be consistent with high-dimensional asymptotic limit, albeit with different coefficients. Calculations of the pair correlation function $g_2(r)$ and structure factor $S(k)$ for these states show that short-range ordering appreciably decreases with increasing dimension, consistent with a recently proposed “decorrelation principle,” which, among other things, states that unconstrained correlations diminish as the dimension increases and vanish entirely in the limit $d \rightarrow \infty$. As in three dimensions (where $\phi_{MRJ} \simeq 0.64$), the packings show no signs of crystallization, are isostatic, and have a power-law divergence in $g_2(r)$ at contact with power-law exponent $\simeq 0.4$. Across dimensions, the cumulative number of neighbors equals the kissing number of the conjectured densest packing close to where $g_2(r)$ has its first minimum. Additionally, we obtain estimates for the freezing and melting packing fractions for the equilibrium hard-sphere fluid-solid transition, $\phi_F \simeq 0.32$ and $\phi_M \simeq 0.39$, respectively, for $d = 4$, and $\phi_F \simeq 0.19$ and $\phi_M \simeq 0.24$, respectively, for $d = 5$. Although our results indicate the stable phase at high density is a crystalline solid, nucleation appears to be strongly suppressed with increasing dimension.

*Electronic address: torquato@electron.princeton.edu

I. INTRODUCTION

Hard-sphere systems are model systems for understanding the equilibrium and dynamical properties of a variety of materials, including simple fluids, colloids, glasses, and granular media. The hard-sphere potential is purely repulsive; it is infinite when two spheres overlap, but otherwise zero. Despite the simplicity of the potential, hard-sphere systems exhibit rich behavior: they undergo a fluid-solid phase transition and can exhibit glassy behavior. Of particular recent interest are (nonequilibrium) disordered jammed packings of hard spheres and their statistical and mechanical properties, such as the maximally random jammed (MRJ) state [1, 2], pair correlations [3], isostaticity [3], and density fluctuations [4]. Such packings have been intensely studied computationally in two and three dimensions [1, 2, 3, 4, 5, 6, 7, 8, 9, 10, 11] and in this paper we extend these studies to four, five and six dimensions.

A hard-sphere packing in d -dimensional Euclidean space \mathbb{R}^d is an arrangement of congruent spheres, no two of which overlap. As in a variety of interacting many-body systems [12], we expect studies of hard-sphere packings in high dimensions to yield great insight into the corresponding phenomena in lower dimensions. Analytical investigations of hard-spheres can be readily extended into arbitrary spatial dimension [13, 14, 15, 16, 17, 20, 21, 22, 23, 24, 25, 26, 27, 28, 29] and high dimensions can therefore be used as a stringent testing ground for such theories. Along these lines and of particular interest to this paper, predictions have been made about long-wavelength density fluctuations [25] and decorrelation [27, 28] in disordered hard-sphere packings in high dimensions. Additionally, the optimal packing of hard spheres in high dimensions is also of interest in error-correcting codes in communications theory [30].

Our focus in this paper will be the study of hard-sphere packings in four, five and six dimensions. Specifically, we consider both equilibrium packings for $d = 4$ and $d = 5$ and nonequilibrium packings representative of the maximally random jammed state for $d = 4$, $d = 5$ and $d = 6$.

Equilibrium thermodynamic properties of hard-sphere packings for $d = 4$ and $d = 5$ have been studied both computationally and with approximate theories [15, 22, 31]. For the low-density fluid, lower-order virial coefficients, B_2 , B_3 , and B_4 , are known exactly for arbitrary dimensionality [13, 14, 17]. Higher-order virial coefficients have been calculated

by Monte Carlo simulation, B_5 , B_6 and B_7 for both $d = 4$ and $d = 5$ [16] and B_8 for $d = 4$ [16], and analytically [18, 19]. The pair correlation function for equilibrium fluids has been studied and a decrease in ordering with increasing dimension was readily apparent [32]. Hard-sphere systems have been shown to undergo a (first-order) fluid-solid phase transition by numerical simulations for $3 \leq d \leq 5$ [33] and with approximate theories for d as high as 50 [22]. The freezing points for $d = 4$ and $d = 5$ were estimated numerically to occur at packing fractions $\phi_F \approx 0.5\phi_{max} = 0.31$ and $\phi_F \approx 0.4\phi_{max} = 0.19$, respectively, and it was conjectured that freezing occurs at lower packing fractions relative to close packing as the dimension increases [33]. The *packing fraction* ϕ is the fraction of space \mathbb{R}^d covered by the spheres, i.e.,

$$\phi = \rho v_1(R), \quad (1)$$

where ρ is the number density,

$$v_1(R) = \frac{\pi^{d/2}}{\Gamma(1 + d/2)} R^d \quad (2)$$

is the volume of a d -dimensional sphere of radius R , and $\Gamma(x)$ is the gamma function [23].

At sufficiently large densities, the packing of spheres with the highest jamming density has the greatest entropy because the free-volume entropy dominates over the degeneracy entropy. Therefore, the high-density equilibrium phase corresponds to the optimal packing, *i.e.*, maximal density. The densest packing for $d = 3$ was recently proven by Hales [34] to be attained by the FCC lattice with packing fraction $\phi_{max} = \pi/\sqrt{18} = 0.7404\dots$. The kissing number Z , the number of spheres in contact with any given sphere, for the FCC lattice corresponds to the maximal kissing number $Z_{max} = 12$ for $d = 3$. One of the generalizations of the FCC lattice to higher dimensions is the D_d checkerboard lattice, defined by taking a cubic lattice and placing spheres on every site at which the sum of the lattice indices is even (*i.e.*, every other site). The densest packing for $d = 4$ is conjectured to be the D_4 lattice, with packing fraction $\phi_{max} = \pi^2/16 = 0.6168\dots$ and kissing number $Z = Z_{max} = 24$ [30], which is also the maximal kissing number in $d = 4$ [35]. For $d = 5$, the densest packing is conjectured to be the D_5 lattice, with packing fraction $\phi_{max} = 2\pi^2/(30\sqrt{2}) = 0.4652\dots$ and kissing number $Z = 40$ [30]. For $d = 6$, the densest packing is conjectured to be the “root” lattice E_6 , with density $\phi_{max} = 3\pi^3/(144\sqrt{3}) = 0.3729\dots$ and kissing number $Z = 72$ [30]. The maximal kissing numbers Z_{max} for $d = 5$ and $d = 6$ are not known, but have the following bounds: $40 \leq Z_{max} \leq 46$ for $d = 5$ and $72 \leq Z_{max} \leq 82$ for $d = 6$ [30]. In very

high dimensions, it has been suggested that random packings of spheres might have a higher density than ordered packings, enabling the intriguing possibility of disordered ground states and hence thermodynamic glass transitions [27]; see also Ref. [28].

Equilibrium hard-sphere systems for $d = 2$ and $d = 3$ crystallize into ordered packings upon densification. However, for $d = 3$, it has been found both experimentally [36] and computationally [1, 3, 5] that if the system is densified sufficiently rapidly, the system can be kept out-of-equilibrium and can jam in a disordered state. A jammed packing is one in which the particle positions are fixed by the impenetrability constraints and boundary conditions, despite thermal or mechanical agitation of the particles or imposed boundary deformations or loads. Depending on the boundary conditions, different jamming categories can be precisely defined, including local, collective and strict jamming [37, 38, 39]. The density of disordered collectively jammed hard-sphere packings for $d = 3$ is around $\phi \simeq 0.64$ for a variety of packing-generation protocols and has traditionally been called random close packing (RCP) [23]. However, Ref. [1] showed that RCP is ill-defined because “random” and “close packed” are at odds with one another and the precise proportion of each of these competing effects is arbitrary. Therefore, Ref. [1] introduced the concept of the maximally random jammed (MRJ) state to be the most disordered jammed packing in the given jamming category. This definition presupposes an order metric ψ can be defined such that $\psi = 1$ corresponds to the most ordered (*i.e.*, crystal) packing and $\psi = 0$ corresponds to the most disordered packing, in which there are no spatial correlations. Figure 1 from Ref. [1] shows where MRJ lies on a schematic diagram of the space of jammed packings in the density-disorder ϕ - ψ plane.

In this paper, we numerically study MRJ packings of hard spheres for $d = 4, 5$ and 6 that are at least collectively jammed and report the first estimates of the packing fractions of the MRJ states [1] in these dimensions to be $\phi_{MRJ} \simeq 0.46, 0.31$ and 0.20 , respectively. We find that short-range ordering exhibited by $g_2(r)$ and $S(k)$ appreciably diminishes with increasing dimension, consistent with a recently proposed “decorrelation principle” stating that unconstrained spatial correlations vanish asymptotically in high dimensions and that the n -particle correlation function g_n for any $n \geq 3$ can be inferred entirely from a knowledge of the number density ρ and the pair correlation function $g_2(\mathbf{r})$ [27, 40]. We also explore equilibrium properties, in particular the fluid-solid phase transition, for $d = 4$ and $d = 5$, and find a decreased tendency to crystallize with increasing dimension.

This paper is organized as follows: Section II explains the simulation procedure, Section

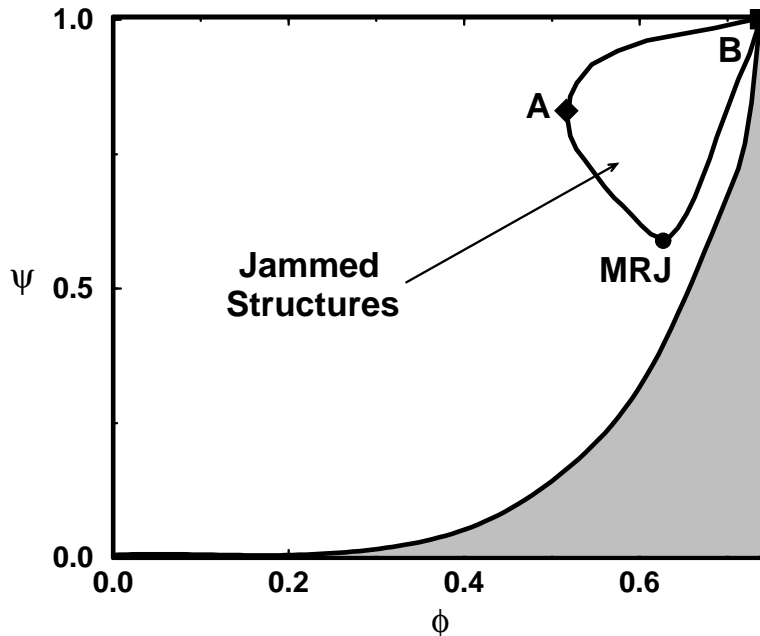


FIG. 1: A highly schematic plot of the subspace in the density-disorder $\phi - \psi$ plane, where strictly jammed three-dimensional packings exist, as adapted from Ref. [1]. Point A corresponds to the lowest-density jammed packing, and it is intuitive to expect that a certain ordering will be needed to produce low-density jammed packings. Point B corresponds to the most dense jammed packing, which is also expected to be the most ordered. Point MRJ represents the maximally random jammed state. The jamming region in the ϕ - ψ plane will of course depend on the jamming category. The gray region is devoid of hard-sphere configurations.

III gives equilibrium results for $d = 4$ and $d = 5$, Section IV gives results for disordered jammed packings for $d = 4, 5$ and 6 , and Section V summarizes and discusses our results.

II. SIMULATION PROCEDURE

We use event-driven molecular dynamics and a modified Lubachevsky-Stillinger (LS) algorithm [41], as in Ref. [42], to produce collectively-jammed hard-sphere packings. As in Ref. [42], our algorithm uses periodic boundary conditions applied to a hypercubic cell, in which a fundamental cell containing N spheres is periodically replicated to fill all of Euclidean space. We also use the cell method, in which the computational domain is di-

vided into cubic cells and only neighboring cells are checked when predicting collisions for a given sphere. Since the number of neighboring cells, as well as the number of spheres per cell, increases considerably with increasing dimension, working in high dimensions is computationally intensive. Additionally, eliminating excessive boundary effects requires on the order of ten sphere diameters per simulation box length, *i.e.*, on the order of $N = 10^d$ spheres. Due to the increasing computational load with increasing dimension, we cannot yet study $d > 6$. Implementing the near-neighbor list (NNL) techniques from Ref. [42], as well as parallelization, are necessary in order to study higher dimensions. Dimension-independent C++ codes used to generate the data in this paper can be downloaded at <http://cherrypit.princeton.edu/Packing/C++/>.

Starting from a Poisson distribution of points, the points grow into nonoverlapping spheres of diameter D at an expansion rate $\gamma = dD/dt$, while the positions of the spheres evolve in time according to Newtonian mechanics, augmented with energy non-conserving collisions. Spheres receive an extra energy boost after the collision due to the positive expansion rate. In practice, the starting configurations for our packing algorithm are low density random-sequential-addition packings of spheres [23]. As the density increases, statistics, such as pressure, are collected. In the limit $\gamma \rightarrow 0$, the system is in equilibrium; for small but nonzero γ , the system is in quasi-equilibrium; and for large γ , the system is out of equilibrium. Eventually, a jammed state with diverging collision rate is reached. For studies of amorphous jammed packings, the expansion must be initially fast to suppress crystallization and maximize disorder, but at sufficiently high pressure, the expansion rate must be slow enough to allow local particle rearrangements necessary to achieve jamming [3].

III. EQUILIBRIUM AND METASTABLE PROPERTIES

The temperature in equilibrium systems of hard spheres is a trivial variable; *i.e.*, it does not affect equilibrium configurational correlations, leaving only one independent thermodynamic state variable, which can be taken to be either the reduced pressure $p = PV/Nk_B T$ or the density ϕ , related through the equation of state (EOS). Hard-sphere systems undergo a (first-order) fluid-solid phase transition, characterized by a melting point, *i.e.*, the density at which the crystal thermodynamically begins to melt, and a freezing point, *i.e.*, the density at which the fluid thermodynamically begins to freeze. Equilibrium properties, such as the

melting and freezing points, are studied here using small expansion rates ($\gamma = 10^{-5} - 10^{-9}$) and periodic rescaling of the average sphere velocity to one, such that the total change in kinetic energy of the system, due to the collisions between growing spheres, was kept small. Strictly speaking, a positive growth rate yields nonequilibrium packings but equilibrium packings result as the growth rate tends to zero. The packings were “equilibrated” by verifying that orders of magnitude of change in the expansion rate did not change the resulting equation of state. In this section we only consider four and five dimensions due to (presently) prohibitive computational costs for higher dimensions.

Figure 2 shows the reduced pressure p as a function of density ϕ for (a) simulations of $d = 4$ systems of spheres placed in a D_4 lattice with negative expansion rate $\gamma = -10^{-6}$ and (b) simulations of $d = 5$ systems of spheres placed in a D_5 lattice with negative expansion rate $\gamma = -10^{-5}$. The pressure initially follows the (lower) crystal branch, until the system becomes mechanically unstable and jumps onto the (higher) fluid branch. Also plotted is the theoretical prediction of Luban and Michels (LM) for the equation of state [15], which agrees well with our numerical results for the fluid branch for $d = 4$, but less so for $d = 5$. It is a computational observation that crystals become mechanically unstable, giving rise to a sudden jump in pressure, at a density close to the freezing point [43, 44]. Such “superheating” (undercompression) is most likely due to the difficulty of achieving coexistence in finite systems, although we are not aware of a theoretical analysis. From the results in Fig. 2, we estimate the freezing points for $d = 4$ and $d = 5$ to be $\phi_F \simeq 0.31 - 0.32$ and $\phi_F \simeq 0.19 - 0.20$, respectively.

The melting points for $d = 4$ and $d = 5$ can also be estimated from the data in Fig. 2. Since throughout the coexistence region the fluid and solid have the same absolute pressure P , the melting density can be estimated as the density on the crystal branch with the same absolute pressure P as that at the freezing point. The coexistence region is plotted in Fig. 2 and the melting packing fractions for $d = 4$ and $d = 5$ are estimated to be $\phi_M \simeq 0.38 - 0.40$ and $\phi_M \simeq 0.24 - 0.26$, respectively. We also observe that the reduced pressure at the freezing point is $p_F \simeq 12$ in both $d = 4$ and $d = 5$, which agrees with the reduced pressure at the freezing point for $d = 3$, $p_F \simeq 12.3$, obtained from free energy calculations [45].

The melting point was also estimated for $d = 4$ (higher dimensions are presently too computationally demanding) by slowly densifying a system of spheres, initially a fluid, and looking for the onset of partial crystallization, again by monitoring the reduced pressure p as

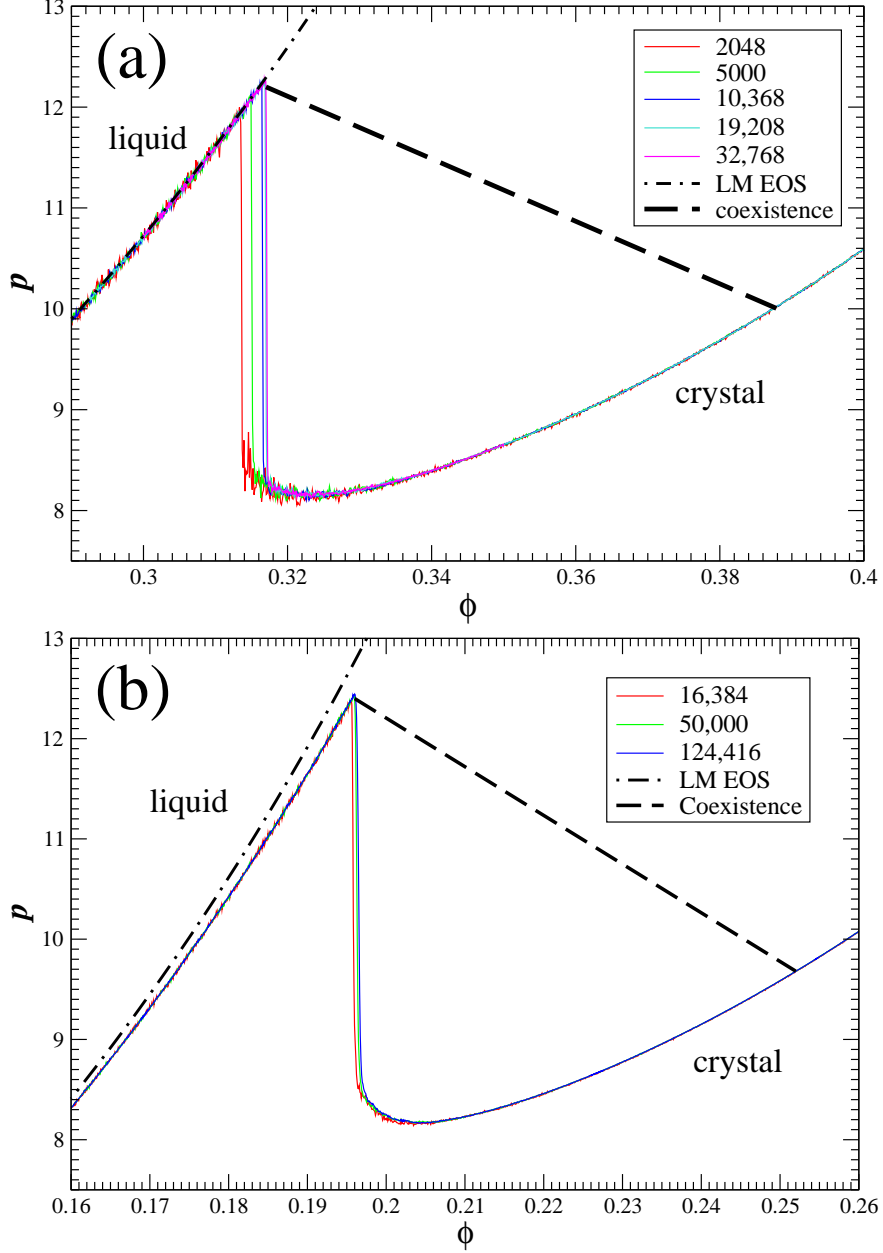


FIG. 2: (Color online) Reduced pressure p as a function of density ϕ , for a range of system sizes (see legend), for (a) $d = 4$ systems of spheres, initially in a D_4 lattice, and negative expansion rate $\gamma = -10^{-6}$ and (b) $d = 5$ systems of spheres, initially in a D_5 lattice, and negative expansion rate $\gamma = -10^{-5}$. N was chosen to make a perfect D_d lattice with periodic boundary conditions, *i.e.*, $N = (2n)^d/2$ for $n \in \mathbb{Z}$. Also plotted is the theoretical prediction of Luban and Michels (LM) for the equation of state [15]. Curves for larger system sizes lie farther to the right.

a function of density ϕ . Due to the difficulty of observing coexistence in finite systems and the relatively high activation barrier, simulated hard-sphere systems become “supercooled” (overcompressed) and nucleation does not occur until the melting density is surpassed. Consequently, the density at which partial crystallization appears for sufficiently slow expansion provides a reasonable estimate for the melting density. Near jamming the reduced pressure is asymptotically given by the free-volume equation of state [46],

$$p = \frac{PV}{Nk_B T} = \frac{1}{\delta} = \frac{d}{1 - \phi/\phi_J}, \quad (3)$$

which can be inverted to give an estimate $\tilde{\phi}_J$ of the jamming density,

$$\tilde{\phi}_J = \frac{\phi}{1 - d/p}. \quad (4)$$

Since the pressure increases very rapidly near jamming, it is more convenient to plot the estimated jamming density $\tilde{\phi}_J(\phi)$ instead of the pressure $p(\phi)$, as shown in Fig. 3 for a system of 648 spheres in $d = 4$. In such a plot, the onset of partial crystallization causes a dramatic jump in $\tilde{\phi}_J(\phi)$, as the jamming density of the crystal is much higher than the jamming density of a disordered packing. The intersection of the curves with the line $\tilde{\phi}_J(\phi) = \phi$ gives the final jamming density. Sufficiently fast expansion suppresses crystallization and leads to packing fractions around 0.45 – 0.47. Slower expansion allows for partial crystallization, typically around $\phi_M \simeq 0.38 - 0.39$, which is our rough estimate of the melting point, in agreement with our estimate from the results in Fig. 2. More accurate estimates can only be obtained using free-energy calculations. Since crystallization is a nucleated process, it is not surprising that the same expansion rates γ can crystallize at different packing fractions and onto different crystal branches, *e.g.* $\gamma = 10^{-8}$ (a) and (b) in Fig. 3.

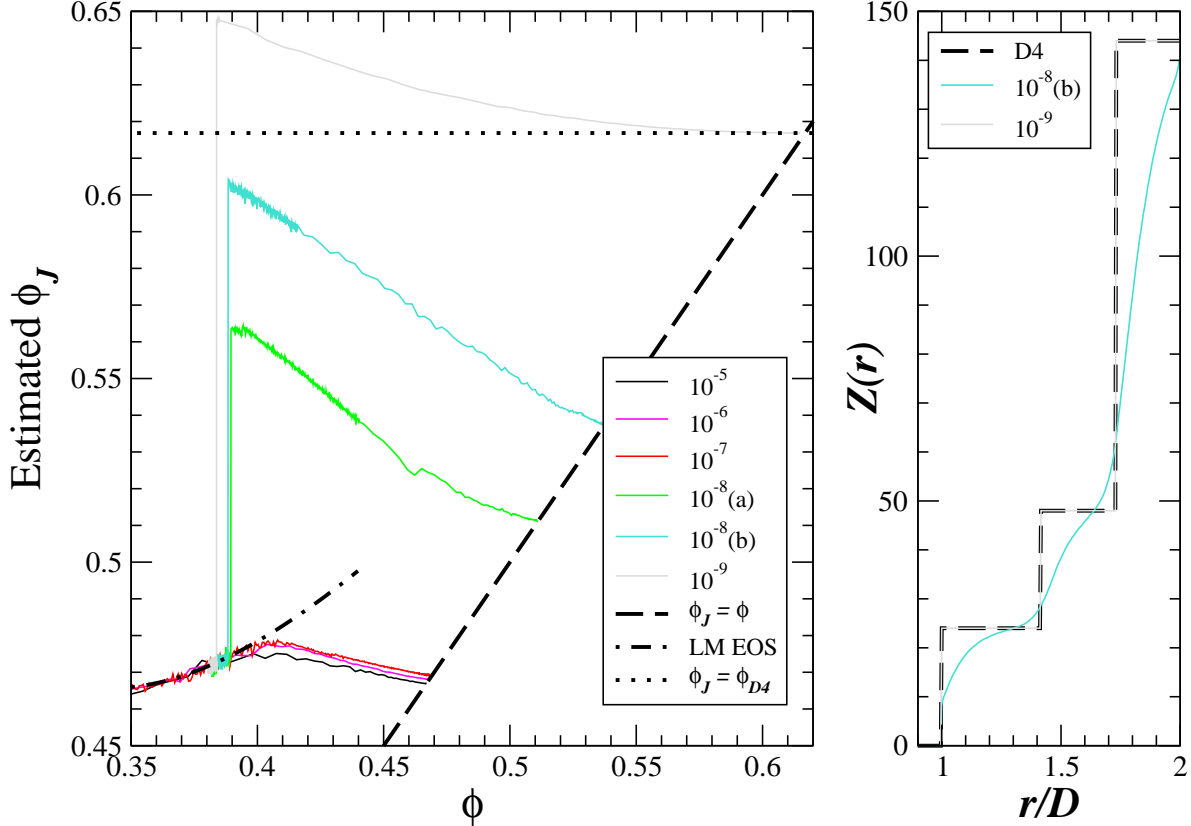


FIG. 3: (Color online) Left panel: The estimated jamming packing fraction $\tilde{\phi}_J$ as a function of density ϕ for systems of 648 spheres for $d = 4$ with various expansion rates (see legend and note that there are two samples labeled (a) and (b) for $\gamma = 10^{-8}$). For the curves showing no partial crystallization (*i.e.*, $\gamma = 10^{-5}$, 10^{-6} , and 10^{-7}), curves with smaller expansion rates have larger peak heights. For the curves that show partial crystallization (*i.e.* $\gamma = 10^{-8}$ (a and b) and 10^{-9}), curves with smaller expansion rate lie farther to the left. Right panel: The cumulative coordination $Z(r)$ (*i.e.*, the number of contacts) for the perfect D_4 lattice and for the partially crystallized packings at $p > 10^{12}$ obtained for expansion rates $\gamma = 10^{-8}$ and $\gamma = 10^{-9}$. The jamming packing fraction for the $\gamma = 10^{-8}$ packing is $\phi = 0.511$, and the jamming packing fraction for the $\gamma = 10^{-9}$ packing agreed up to 12 significant figures with the density of the D_4 lattice, $\phi = \pi^2/16 \simeq 0.617$.

To determine whether the crystallized packings were forming a D_4 lattice, the conjectured densest packing in four dimensions, we computed the average cumulative coordination number $Z(r)$, which is the average number of sphere centers within a distance r from a given

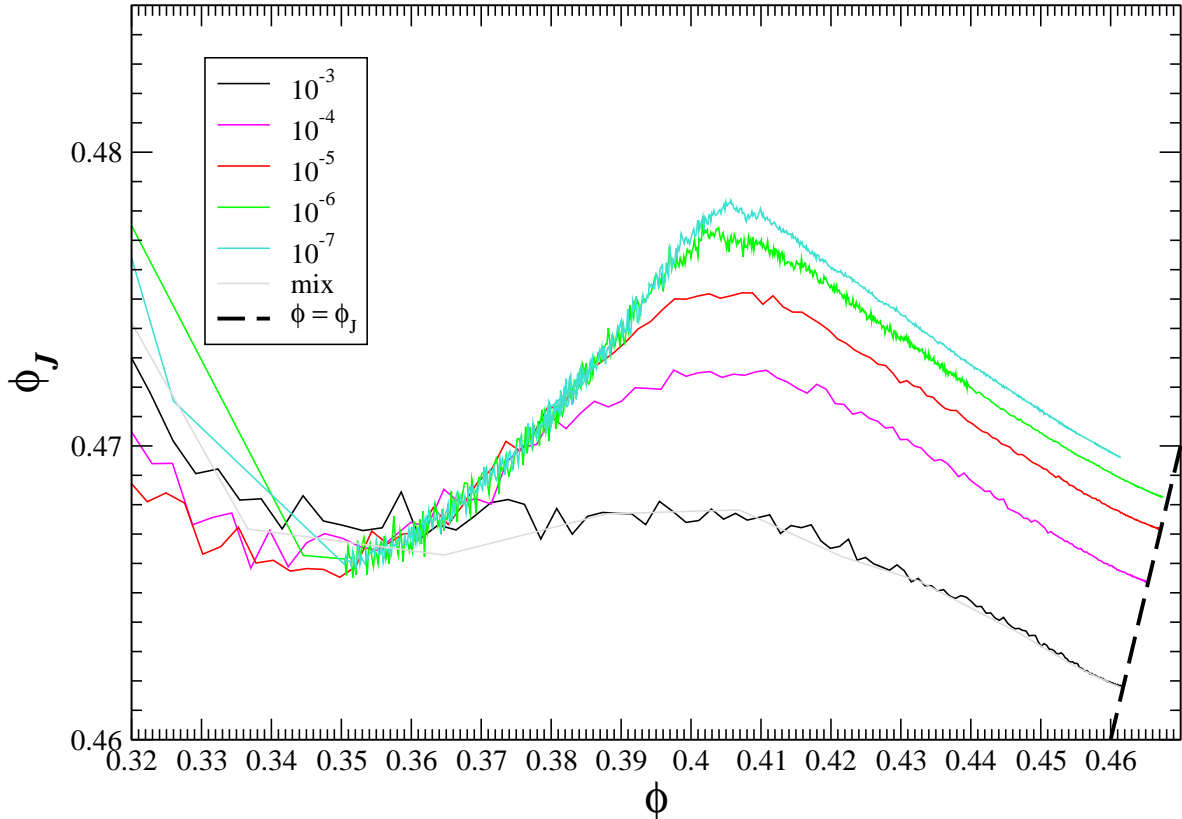


FIG. 4: The estimated jamming packing fraction $\tilde{\phi}_J$ as a function of density ϕ for a system of 10,000 spheres for $d = 4$ with various expansion rates. Curves with smaller expansion rates have larger peak heights. The curve labeled “mix” corresponds to the following sequence of expansion rates: $\gamma = 10^{-2}$ until $p = 10$, $\gamma = 10^{-3}$ until $p = 10^4$, $\gamma = 10^{-4}$ until $p = 10^6$, and $\gamma = 10^{-5}$ until $p = 10^{12}$.

sphere center. The inset to Fig. 3 shows $Z(r)$ for a perfect D_4 lattice and for the crystallized packings with $\gamma = 10^{-8}$ and $\gamma = 10^{-9}$ (corresponding colors represent the same packing). The sharp plateaus for the D_4 lattice correspond to the coordination shells and the number of spheres in the first shell is the kissing number $Z_{max} = 24$. The packing shown with $\gamma = 10^{-9}$ formed a perfect D_4 lattice. The packing shown with $\gamma = 10^{-8}$ partially crystallized with a final density of $\phi \simeq 0.511$.

Figure 4 shows the estimated jamming packing fraction $\tilde{\phi}_J$, as in Fig. 3, but for a system of 10,000 spheres, instead of 648 spheres, in four dimensions. In contrast to the 648 sphere system, there is no sign of partial crystallization for the 10,000-sphere system. In fact, molecular dynamics was performed at packing fractions of $\phi \simeq 0.38 - 0.42$ for 10 mil-

lion collisions per sphere and there was no significant drop in pressure indicative of partial crystallization. The curves in Figs. 3 and 4 exhibit a bump around $\phi_G \simeq 0.41$, suggesting a kinetic transition from the fluid branch to a glassy branch.

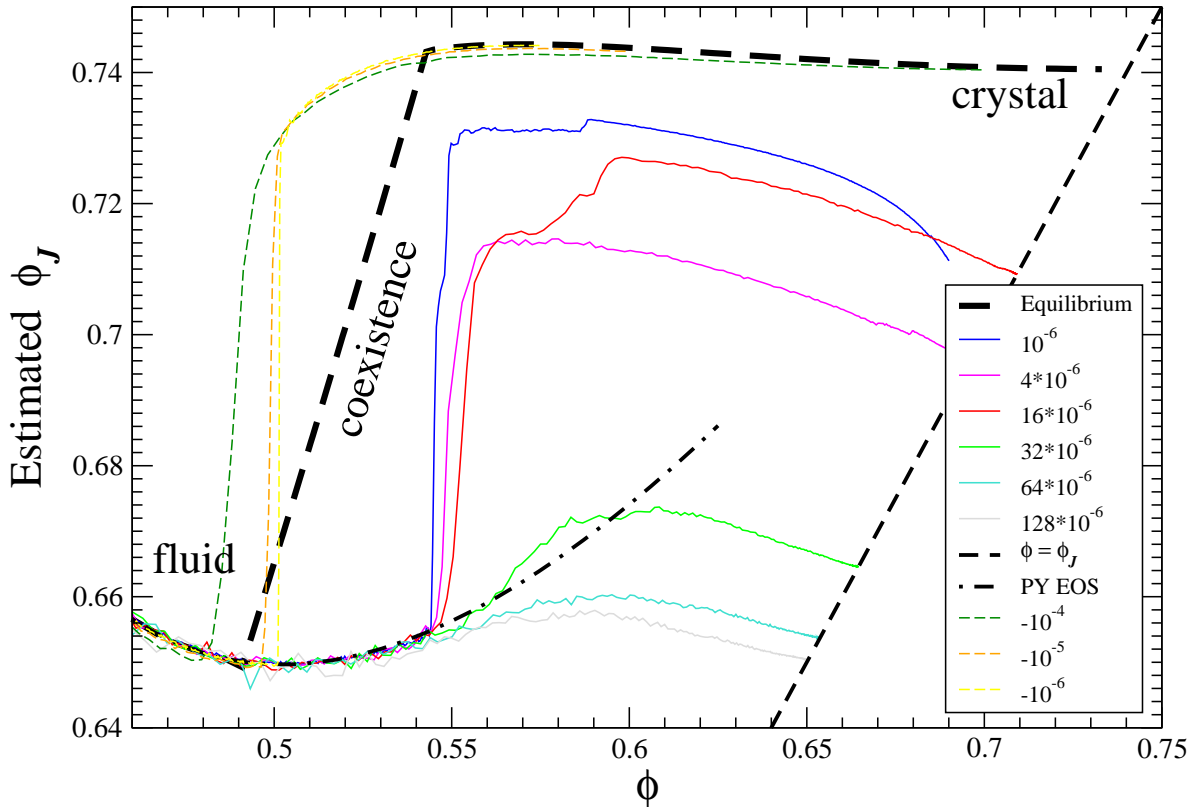


FIG. 5: (Color online) The estimated jamming packing fraction $\tilde{\phi}_J$ as a function of packing fraction ϕ for $d = 3$. Shown are systems of 4096 spheres with various expansion rates and systems of 10,976 spheres placed in an FCC lattice with negative expansion rates $\gamma = -10^{-4}$, -10^{-5} , and -10^{-6} (last three curves). Also plotted are approximations to the equilibrium EOS for the fluid phase, the coexistence region, and the crystal phase [47], as well as the Percus-Yevick (PY) EOS for the fluid phase. Compare this figure to the curves shown in Figs. 3 and 4. For the curves showing no partial crystallization (*i.e.*, $\gamma = 32 \times 10^{-6}$, 64×10^{-6} , and 128×10^{-6}), curves with smaller expansion rates have larger peak heights. For the curves that show partial crystallization (*i.e.*, $\gamma = 10^{-6}$, 4×10^{-6} , and 16×10^{-6}), curves with smaller expansion rates lie farther to the left. For the melting curves (*i.e.*, $\gamma = -10^{-4}$, -10^{-5} , and -10^{-6}), curves with smaller compression rates lie farther to the right.

Figure 5 shows the estimated jamming packing fraction $\tilde{\phi}_J$ for systems of spheres for

$d = 3$ with various positive and negative expansion rates, for comparison with the results for $d = 4$ and $d = 5$ in Figs. 2, 3 and 4. The locations of the freezing and melting points in $d = 3$ have been determined from free-energy calculations [45] and good approximations to the EOS for both the fluid and crystal phases are known [47]. Our estimates of the freezing and melting points as the densities at the onset of melting of a diluted crystal or of partial crystallization of a densified fluid, respectively, compare favorably to the true values computed from free-energy calculations in $d = 3$. The bump around $\phi_G \simeq 0.59$, analogous to the bump in Fig. 4 around $\phi_G \simeq 0.41$, is often cited as the approximate location of the “kinetic” glass transition [48]. Comparing Figs. 4 and 5 reveals that the melting point and suggested kinetic glass transition are closer for $d = 4$ than for $d = 3$, which is a possible reason why there is a lower tendency to crystallize for $d = 4$ than for $d = 3$. Similar results have been observed for binary hard disks, a model glass former [6].

IV. DISORDERED JAMMED PACKINGS

Packings representative of the maximally random jammed (MRJ) state are produced by a combination of expansion rates. The expansion rate must be initially high (compared to the average thermal velocity) to suppress crystallization and produce disordered configurations that are trapped in the neighborhood of a jammed packing. Near the jamming point, the expansion rate must be sufficiently slow to allow for particle readjustments necessary for collective jamming. Figure 4 shows the final jamming packing fractions of packings created using a variety of expansion rates, as the packing fraction at which the curves intersect the line $\tilde{\phi}_J = \phi$. We see that by increasing the expansion rate, we attain packings with lower jamming packing fractions.

By comparing Fig. 4 and to the analogous plot for a $d = 3$ system (Fig. 5), where it is widely accepted that $\phi_{MRJ} \simeq 0.64 - 0.65$ [1, 2], we estimate the MRJ density for $d = 4$ to be $\phi_{MRJ} \simeq 0.460 \pm 0.005$. A more accurate calculation of ϕ_{MRJ} demands a better theoretical understanding of order metrics and how the expansion rate in the algorithm affects the ordering in the produced packings; statistical errors are smaller than the effect of the packing-generation protocol. Systematic investigation of different protocol parameters, as done for $d = 4$ in Fig. 4, is currently too computationally intensive in higher dimensions. Reasonable estimates of ϕ_{MRJ} for both $d = 5$ and $d = 6$ are obtained using the following

less computationally intensive procedure. First, the system of spheres is expanded, starting from zero initial kinetic energy ($T = 0$), until it reached a high pressure (say, $p = 100 - 1000$). Then the system is slowly expanded ($\gamma = 10^{-5} - 10^{-3}$) and periodically cooled to $k_B T = 1$ until a very high pressure (say, $p = 10^{12}$) is attained. The resulting packings are approximately collectively jammed, as demonstrated by very large relaxation times for the pressure during long molecular dynamics runs [3]. Using this method we estimate the MRJ density for $d = 5$ to be $\phi_{MRJ} \simeq 0.310 \pm 0.005$ and for $d = 6$ to be $\phi_{MRJ} \simeq 0.200 \pm 0.01$.

The MRJ packing fractions as well as important equilibrium packing fractions are summarized in Table I. It is useful to compare the MRJ packings fractions for $3 \leq d \leq 6$ to recent estimates of the *saturation* packing fraction ϕ_s for the random sequential addition (RSA) packing of hard spheres obtained by Torquato, Uche and Stillinger [29] in corresponding dimensions, which were shown to be nearly hyperuniform [25]. These authors found that $\phi_s = 0.38278 \pm 0.000046, 0.25454 \pm 0.000091, 0.16102 \pm 0.000036$ and 0.09394 ± 0.000048 for $d = 3, 4, 5$ and 6 , respectively. The nonequilibrium RSA packing is produced by randomly, irreversibly, and sequentially placing nonoverlapping spheres into a volume. As the process continues, it becomes more difficult to find available regions into which the spheres can be added. Eventually, in the saturation (infinite-time) limit, no further additions are possible, and the maximal achievable packing fraction is the saturation value ϕ_s [see Ref. [23] and references therein]. As expected, the RSA saturation packing fraction in dimension d is substantially smaller than the corresponding MRJ value because, unlike the latter packing, the particles cannot rearrange.

Our estimates for the MRJ packing fraction are compared to a theoretical formula proposed by Philipse [24] for the “random jamming density” ϕ_d ,

$$\phi_d \simeq \frac{0.046d^2 + 1.22d + 0.73}{2^d}, \quad (5)$$

which predicts $\phi_3 \simeq 0.601$, $\phi_4 \simeq 0.397$, $\phi_5 \simeq 0.249$, and $\phi_6 \simeq 0.152$. It is seen that Eq. (5) underestimates MRJ density ϕ_{MRJ} in $d = 3$ and becomes worse with increasing dimension. Following Ref. [29], we obtain a better scaling form by noting that the product $2^d \phi_{MRJ}$ for $3 \leq d \leq 6$ is well approximated by a function linear, rather than quadratic, in d (see Fig. 6), i.e., the scaling form for ϕ_{MRJ} is given by

$$\phi_{MRJ} = \frac{c_1}{2^d} + \frac{c_2 d}{2^d}, \quad (6)$$

Packing fraction	$d = 3$	$d = 4$	$d = 5$	$d = 6$
ϕ_F	0.494 [23, 45]	$0.32 \pm 0.01^*$	$0.19 \pm 0.01^*$	-
ϕ_M	0.545 [23, 45]	$0.39 \pm 0.01^*$	$0.24 \pm 0.01^*$	-
ϕ_{MRJ}	0.645 ± 0.005 [2]	$0.46 \pm 0.005^*$	$0.31 \pm 0.005^*$	$0.20 \pm 0.01^*$
ϕ_{max}	0.7405... [34]	0.6169... [30]	0.4652... [30]	0.3729... [30]

TABLE I: Important packing fractions for $d = 3, 4, 5$ and 6 . These include the equilibrium values for the freezing, ϕ_F , melting, ϕ_M , and densest states, ϕ_{max} , as well as the nonequilibrium MRJ values. The freezing and melting points for $d = 6$ were not calculated here. *Values computed in this work.

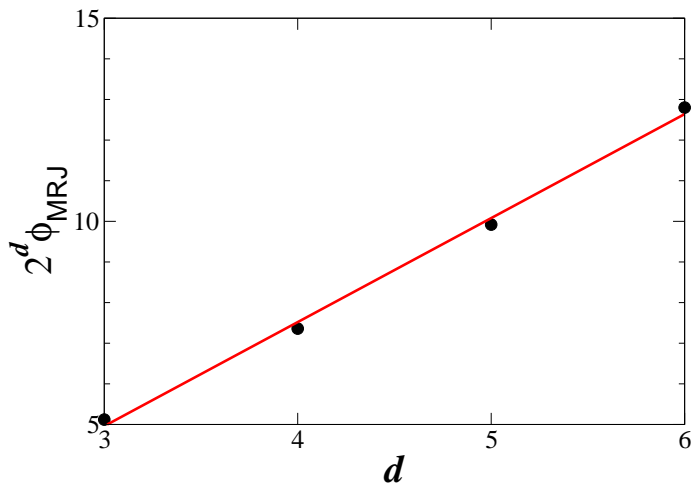


FIG. 6: (Color online) Fit of the data for the product $2^d \phi_{MRJ}$ to the linear form (6) for $3 \leq d \leq 6$ with $c_1 = -2.72$ and $c_2 = 2.56$.

where $c_1 = -2.72$ and $c_2 = 2.56$. Although the scaling form (6) applies only in low dimensions such that $d \geq 3$, theoretical arguments given by Torquato, Uche and Stillinger [29] suggest that the general scaling form (6) persists in the high-dimensional asymptotic limit, albeit with different coefficients c_1 and c_2 . In Ref. [29], the density lower bound $\phi_{MRJ} \geq (d+2)/2^d$ is derived for MRJ packings in any dimension. This MRJ density lower bound yields 0.3125, 0.1875, 0.109375, 0.0625 for $d = 3, 4, 5$ and 6 , respectively. We note that Parisi and Zamponi [26] suggest the MRJ density scaling $\phi_{MRJ} \sim (d \log d)/2^d$.

A. Pair Correlations

Our main interest is pair correlations in the jamming limit in four, five and six dimensions. We characterize jammed packings statistically using the pair correlation function $g_2(r)$ and structure factor $S(k)$. The pair correlation function measures the probability of finding a sphere center at a given distance from the center of another sphere, normalized by the average number density ρ to go asymptotically to unity at large r ; *i.e.*

$$g_2(r) = \frac{\langle P(r) \rangle}{\rho s_1(r)}, \quad (7)$$

where $P(r)$ is the probability density for finding a sphere center a distance r from an arbitrary sphere center, $\langle \rangle$ denotes an ensemble average, and $s_1(r)$ is the surface area of a single hypersphere of radius r [23]: $s_1(r) = 2\pi^2 r^3$ in $d = 4$, $s_1(r) = 8\pi^2 r^4/3$ in $d = 5$ and $s_1(r) = \pi^3 r^5$ in $d = 6$. The structure factor

$$S(k) = 1 + \rho \hat{h}(k) \quad (8)$$

is related to the Fourier transform of the total correlation function $h(r) = g_2(r) - 1$. It measures spatial correlations at wavenumber k and in particular, large-scale density fluctuations at $k = 0$ [25]. The structure factor can be observed directly via scattering experiments [12].

In the jamming limit, the pair correlation function $g_2(r)$ consists of a δ -function due to sphere contacts and a background part $g_2^b(r)$ due to spheres not in contact:

$$g_2(r) = \frac{\bar{Z}\delta(r - D)}{\rho s_1(D)} + g_2^b(r), \quad (9)$$

where \bar{Z} is the average kissing number. Figure 7 compares the pair correlation function for jammed packings of 10^5 spheres in $d = 3, 4, 5$ and 6 . Due to periodic boundary conditions, $g_2(r)$ can only be calculated up to half the length of the simulation box, which limits the calculation to $r/D \simeq 3$ for $d = 6$. The well-known split second peak present in $d = 3$ is strongly diminished as the dimension increases, *i.e.*, the amplitude of the split second peak decreases and the sharp cusps become rounded with increasing dimension. The split third peak present in $d = 3$ with considerable structure and two shoulders vanishes almost completely in the higher dimensions. The oscillations are strongly damped with increasing dimension and the period of oscillations might also decrease slightly with increasing dimension; this latter possibility is revealed more vividly in the structure factor through the shift

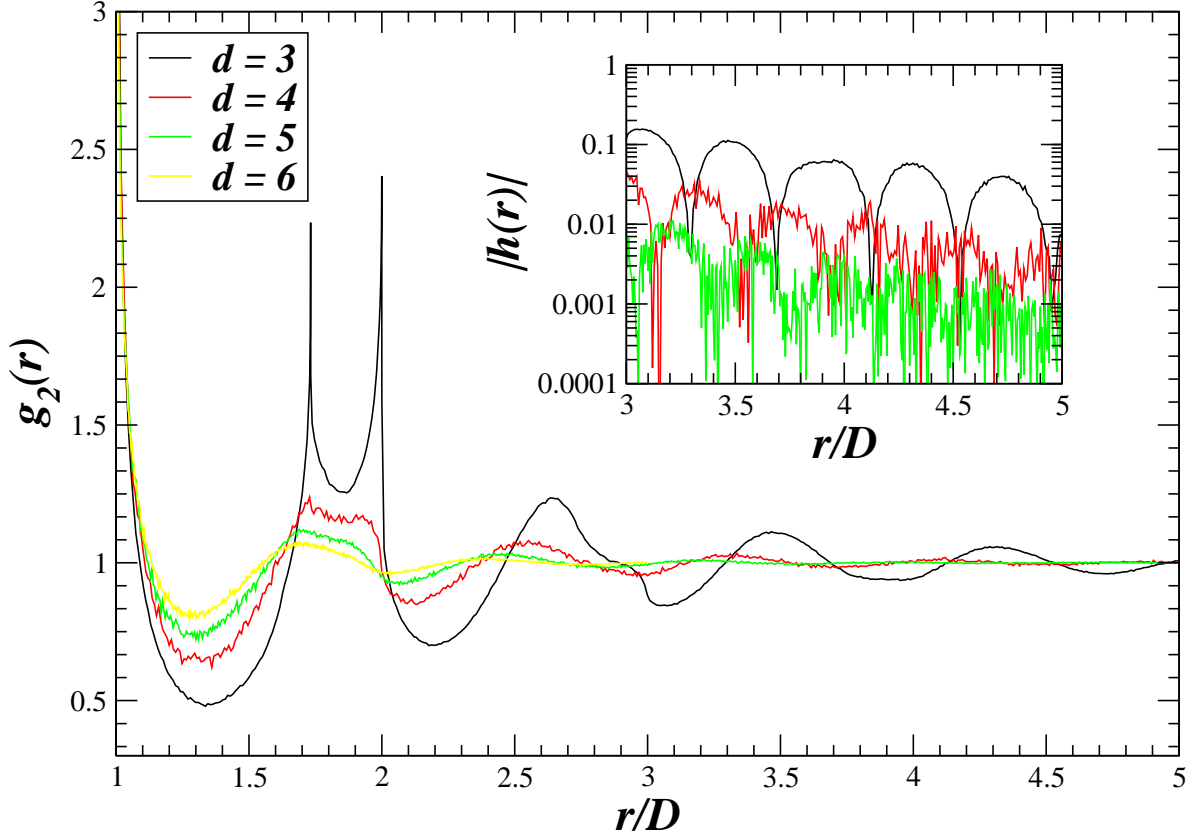


FIG. 7: The pair correlation function $g_2(r)$ for MRJ packings of 10^4 hard spheres for $d = 3, 4, 5$ and 6 at the respective densities reported in Table I. Pair separation is plotted in units of the sphere diameter D . [For $d = 6$, $g_2(r)$ was only calculated up to $r/D = 3$ due to the system size and periodic boundary conditions]. The delta-function contribution [cf. Eq. 9] at contact, of course, is not shown. The inset shows $|h(r)| = |g_2(r) - 1|$ on a logarithmic scale for $d = 3, 4$ and 5 . Each curve for $g_2(r)$ is obtained from a single packing realization (not time-averaged). Curves for higher dimensions are increasingly diminished.

in the location of the maximum, as we will describe below. The inset to Fig. 7 shows the magnitude of the decaying oscillations in $h(r)$ on a semi-log scale. Though at the values of r/D shown, up to about half the length of the simulation box, there is still structure in addition to the oscillations, especially apparent for $d = 3$, it appears that the decay rate of the oscillations in $h(r)$ does not change significantly with dimension, whereas the amplitude of oscillations does. However, further studies with larger r and therefore larger systems are needed to obtain more quantitative results.

We calculate the structure factor $S(k)$, defined in Eq. 8, for $d = 4$ and $d = 5$ by

$$S(K) = 1 + 128\phi \int_0^\infty x^3 h(x) \frac{J_1(Kx)}{Kx} dx \quad (10)$$

and

$$S(K) = 1 + 480\phi \int_0^\infty \frac{x^4 h(x)}{(Kx)^2} \left[\frac{\sin(Kx)}{Kx} - \cos(Kx) \right] dx, \quad (11)$$

respectively, where $\phi = \pi^2 \rho D^4 / 32$ for $d = 4$ and $\phi = \pi^2 \rho D^5 / 60$ for $d = 5$, $x = r/D$ and $K = kD$ are the dimensionless radius and wave number, and $J_\nu(x)$ is the Bessel function of order ν . We do not calculate the structure factor for $d = 6$ because at present we do not have $g_2(r)$ over a sufficiently large range of r .

Following Ref. [4], rather than working directly with $g_2(x)$ as in Eq. (8), we consider the average cumulative coordination $Z(x)$, defined to be the following volume integral of $g_2(x)$:

$$Z(x) = \rho \int_1^x s_1(x') g_2(x') dx'. \quad (12)$$

The excess coordination $\Delta Z(x)$,

$$\Delta Z(x) = 1 + 64\phi \int_0^x (x')^3 h(x') dx' \quad (13)$$

$$\Delta Z(x) = 1 + 160\phi \int_0^x (x')^4 h(x') dx', \quad (14)$$

for $d = 4$ and $d = 5$, respectively, is the average excess number of sphere centers inside a spherical window of radius x centered at a sphere, compared to the ideal gas expectations, $16\phi x^4$ for $d = 4$ and $32\phi x^5$ in $d = 5$. We can rewrite Eq. (8) in terms of $\Delta Z(x)$ using integration by parts to get

$$S(K) = -2 \int_0^\infty \Delta Z(x) \frac{d}{dx} \frac{J_1(Kx)}{Kx} dx \quad (15)$$

and

$$S(K) = -3 \int_0^\infty \Delta Z(x) \frac{d}{dx} \left[\frac{\sin(Kx)}{(Kx)^3} - \frac{\cos(Kx)}{(Kx)^2} \right] dx, \quad (16)$$

for $d = 4$ and $d = 5$, respectively. Note that accurate evaluations of the integrals of $\Delta Z(x)$ require extrapolations of its large- x tail behavior, for which we have used an exponentially-damped oscillating function [49].

Figure 8 shows $S(k)$ for jammed packings of 10^5 spheres in three, four and five dimensions. Qualitatively, $S(k)$ is somewhat similar for $d = 3, 4$, and 5 . However, with increasing dimension, the height of the first peak of $S(k)$ decreases, the location of the first peak

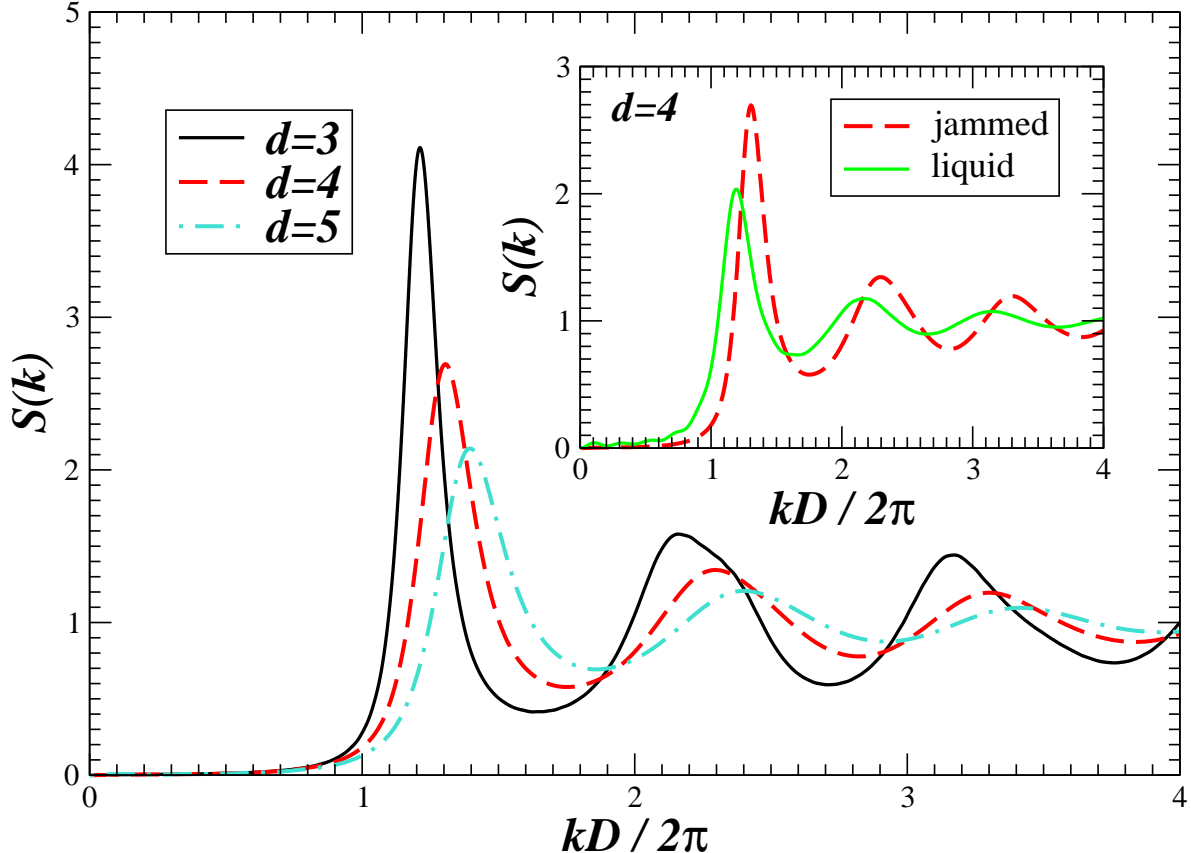


FIG. 8: The structure factor $S(k)$ for jammed packings of 10^5 spheres for $d = 3, 4$ and 5 at the respective densities reported in Table I. Inset: A comparison for $d = 4$ of $S(k)$ for a jammed packing and for a fluid near the freezing point ($\phi \approx 0.31$). Each curve for $S(k)$ is obtained from a single packing realization (not time averaged).

moves to smaller wavelengths, and the oscillations become damped. The width of the first peak also increases with increasing dimension, which could indicate that the correlation length decreases with increasing dimension. The inset to Fig. 8 shows $S(k)$ for a jammed packing and a fluid near the freezing point in four dimensions. The relation between the structure factor for the fluid and jammed packing is strikingly similar to what is found for $d = 3$, except that the peaks of both curves for $d = 4$ appear scaled down relative to $d = 3$. Overall, our results for both $g_2(r)$ and $S(k)$ are consistent with a recently proposed “decorrelation” principle [27]. We note that similar pair decorrelations are observed for RSA packings as the dimension increases up to $d = 6$ [29].

It is of interest to determine whether infinite-wavelength density fluctuations $S(k = 0)$

vanish; systems with this property are called “hyperuniform” [25]. For equilibrium fluids and crystals, $S(k=0)$ is proportional to the isothermal compressibility and therefore must be positive. As for $d=3$, $S(k)$ for $d=4$ appears to go to zero faster near the origin for the jammed packing than for the fluid. However, we cannot reliably determine whether $S(k)$ vanishes at the origin because our calculation of $S(k)$ for small k involved an extrapolation of the large- x tail of $\Delta Z(x)$. Nevertheless, using larger system sizes of one million spheres, saturated [50] MRJ packings for $d=3$ have been shown to be hyperuniform to a high accuracy [4] and the comparison of $d=4$ and $d=5$ to $d=3$, shown in Fig. 8, suggests that MRJ packings for $d=4$ and $d=5$ are also hyperuniform.

B. Isostaticity

We study the near-contact contribution to $g_2(r)$, *i.e.*, interparticle distances r that are very close to the sphere diameter D , using the cumulative coordination number $Z(x)$, where as before $x = r/D$ is the dimensionless radius and $x - 1$ is the dimensionless interparticle gap. Figure 9 shows $Z(x)$ for jammed packings of 10,000 spheres for $d=4$ and $d=5$ with rattlers removed [51]. The plateaus at $Z=8$ in Fig. 9 (a) and $Z=10$ in Fig. 9 (b) show that both packings are isostatic. Isostatic packings are jammed packings which have the minimal number of contacts necessary for collective jamming. For spheres, this occurs when the number of degrees of freedom equals the number of contacts (or constraints); each d -dimensional sphere has d degrees of freedom, and hence the mean number of contacts experienced by a sphere necessary for jamming is $2d$, since each contact involves two spheres.

Packings produced by the LS algorithm almost always contain a nonzero fraction of “rattlers”, which are spheres trapped in a cage of jammed neighbors, but free to move within the cage. We find approximately $\sim 1\%$ rattlers for $d=4$ and $\sim 0.6\%$ rattlers for $d=5$, as compared to $\sim 2-3\%$ rattlers for $d=3$ [3]. Rattlers can be identified as having less than the required $d+1$ contacts necessary for local jamming and are removed to study the jammed backbone of the packing, which we focus on in this section.

The insets to Fig. 9 (a) and (b) show $Z(x) - 2d$, along with a power-law fit for intermediate interparticle gap $x - 1$,

$$Z(x) = \bar{Z} + Z_0(x - 1)^\alpha, \quad (17)$$

where $\bar{Z} = 2d$. Since the packings are generally slightly subisostatic, we apply a small

correction ($< 0.1\%$) to the isostatic prediction of $2d$ by using the midpoint of the apparent plateau in $Z(x)$. The best-fit exponent is $\alpha \simeq 0.6$ in both $d = 4$ and $d = 5$, in agreement with that found for $d = 3$ [3]. The coefficients of the power law, $Z_0 \simeq 11$ in $d = 3$, $Z_0 \simeq 24$ for $d = 4$, and $Z_0 \simeq 40$ for $d = 5$ are close to the corresponding kissing numbers of the densest packings, $Z = 12$ for $d = 3$, $Z = 24$ for $d = 4$, $40 \leq Z \leq 46$ for $d = 5$ and $72 \leq Z \leq 80$ for $d = 6$. Motivated by this observation, we measured the value of the gap $x - 1$ at which the cumulative coordination $Z(x)$ equals the kissing number of the densest packing to be: $x - 1 \simeq 0.35, 0.34, 0.31 - 0.36$ and $0.33 - 0.36$ in $d = 3, 4, 5$ and 6 , respectively, which we can define to be the cutoff for the near-neighbor shell. This definition produces results similar to that of the more common definition of the cutoff for the near-neighbor shell as the value of the gap $x - 1$ at the first minimum in g_2 , which occurs at $x - 1 \simeq 0.35, 0.32, 0.30$ and 0.28 in $d = 3, 4, 5$ and 6 , respectively. It is also interesting to observe that the power-law fit to $Z(x)$ is good over a rather wide range of gaps, almost up to the first minimum in g_2 . We should, however, emphasize that the minimum of g_2 is not very precisely defined, especially due to decorrelation in high dimensions, and the choice of the gap at the minimum of g_2 , or at which $Z(x)$ equals the kissing number of the densest packing, as a special point is somewhat arbitrary and not theoretically justified at present.

V. DISCUSSION

We have presented the first numerical results characterizing random jammed hard-sphere packings in four, five and six dimensions. We find disordered packings, representative of the maximally random jammed state, to be isostatic and have packing fractions $\phi_{MRJ} \simeq 0.46$, $\phi_{MRJ} \simeq 0.31$ and $\phi_{MRJ} \simeq 0.20$ for $d = 4, 5$ and 6 , respectively. For equilibrium sphere packings, we estimate the freezing and melting packing fractions for the fluid-solid transition in four dimensions to be $\phi_F \simeq 0.32$ and $\phi_M \simeq 0.39$, respectively, and in five dimensions to be $\phi_F \simeq 0.19$ and $\phi_M \simeq 0.24$, respectively. Additionally, a signature characteristic of the kinetic glass transition is observed around $\phi_G \simeq 0.41$ for $d = 4$. We observe a significantly lower tendency to crystallize for $d = 4$ than in $d = 3$, which is likely due to the closer proximity of the melting and kinetic glass transition densities for $d = 4$ [6].

We find that in high dimensions the split-second peak in the pair correlation function g_2 , present for $d = 3$, gets dramatically diminished and oscillations in both g_2 and the structure

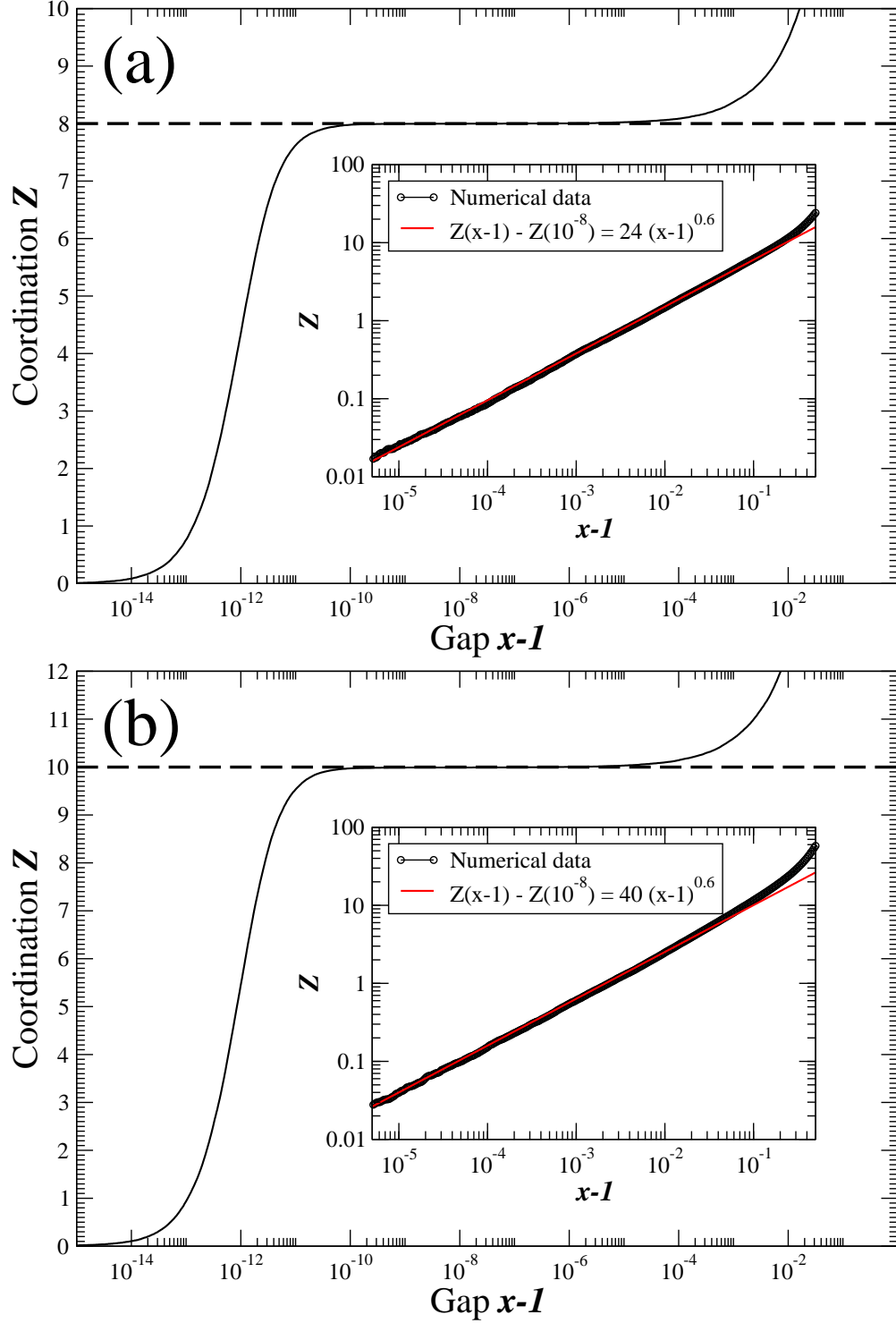


FIG. 9: The near-contact cumulative coordination $Z(x)$ [*c.f.* Eq. 12] for 10^4 -sphere MRJ packings for $d = 4$ (a) and for $d = 5$ (b), with rattlers removed. The inset shows $Z(x)$ on a log-log scale along with power-law fits for intermediate interparticle gap $x - 1$ beyond contact. 10^5 -sphere MRJ packings in $d = 5$ with final expansion rates of $\gamma = 10^{-4}$ give similar results; such packings with final expansion rates of $\gamma = 10^{-5}$ are (presently) too computationally expensive. Compare these plots to the equivalent results for $d = 3$ in Ref.²⁸ [*c.f.* Fig. 8].

factor $S(k)$ get significantly dampened. These findings are consistent with a recently proposed “decorrelation principle” [27], stating that unconstrained spatial correlations vanish asymptotically in the high-dimensional limit and that the n -particle correlation function g_n for any $n \geq 3$ can be inferred entirely from a knowledge of the number density ρ and the pair correlation function $g_2(\mathbf{r})$. Accordingly, in this limit the pair correlation function $g_2(r)$ would be expected to retain the delta-function contribution from nearest-neighbor contacts, but the extra structure representing unconstrained spatial correlations beyond a single sphere diameter would vanish. Figures 7 and 8 show dramatically the decorrelation principle already taking effect in four, five and six dimensions. We note that decorrelation principle is also apparent in the same dimensions for RSA packings [29].

One should not be misled to believe that the decorrelation principle is an expected “mean-field” behavior. For example, it is well known that in some spin systems correlations vanish in the limit $d \rightarrow \infty$ and the system approaches the mean-field behavior. While this idea has meaning for spin systems with attractive interactions, hard-core systems, whose total potential energy is either zero or infinite, cannot be characterized by a mean field. Mean-field theories are limited to equilibrium considerations, and thus do not distinguish between “constrained” and “unconstrained” correlations because, unlike us, they are not concerned with non-equilibrium packings of which there are an infinite number of distinct ensembles. The decorrelation principle is a statement about any disordered packing, equilibrium or not. For example, contact delta functions are an important attribute of non-equilibrium jammed disordered packings and have no analog in equilibrium lattice models of any dimension. The decorrelation principle is also justified on the basis of a rigorous upper bound on the maximal packing density in high dimensions [27], which has no counterpart in mean-field theories.

A particularly interesting property of jammed hard-sphere packings is hyperuniformity, the complete suppression of infinite wavelength density fluctuations, *i.e.*, the vanishing of the structure factor $S(k)$ as $k \rightarrow 0$. It has been recently conjectured that all saturated strictly-jammed packings are hyperuniform [25] and calculations of the structure factor near $k = 0$ for $d = 3$ using one million particle systems have strongly suggested that MRJ packings for $d = 3$ are indeed hyperuniform [4]. Though the system sizes used in this paper were too small to probe such large-scale density fluctuations without relying on dubious extrapolations, our numerical results for the structure factor for $d = 4$ and $d = 5$, as shown

in Fig. 8, are consistent with hyperuniformity.

As in three dimensions, disordered jammed sphere packings show no signs of crystallization, are isostatic, and have a power-law divergence in $g_2(r)$ at contact. Interestingly, all three dimensions (3, 4 and 5) share the same power law exponent $1 - \alpha \simeq 0.4$ when rattlers are removed, and show the first minimum of $g_2(r)$ close to where the cumulative coordination $Z(r)$ equals the kissing number of the densest lattice packing. Such a relation between the kissing numbers of the densest packings and MRJ packings for $d = 3, 4, 5$ and 6, if not coincidental, is very surprising and may be a consequence of the geometrical structure of MRJ packings. It suggests that disordered packings might be deformed crystal packings, in which the true contacts are deformed into near contacts, and only the minimal number of contacts necessary for jamming is preserved. This interpretation is to be contrasted with the usual interpretation of disordered packing in $d = 3$ in terms of tetrahedral or icosahedral packings, without relation to the crystal (FCC) packing. The former interpretation is similar to the one of the MRJ state for binary hard disks as a random partitioning of the monodisperse triangular crystal into “small” and “large” disks, i.e., a deformed monodisperse triangular disk crystal in which a randomly chosen fraction of the particles have grown in size, as proposed in Ref. [6].

It is important to point out that hard-sphere packings behave rather differently in two dimensions than in three and higher dimensions. For $d = 2$, jammed hard-sphere systems are polycrystalline and there is a very weak, nearly continuous fluid-solid phase transition. Hence, there is no glassy behavior for $d = 2$ and consequently no amorphous jammed packings. Glassy behavior, due to geometrical frustration arising from the inconsistency of local optimal packing rules and global packing constraints, first appears in three dimensions [23]. It is likely that geometrical frustration generally increases with dimension, consistent with our observation that nucleation is suppressed with increasing dimension.

Computational costs rise dramatically with increasing dimension and theoretical understanding based on observations in moderate dimensions is necessary. We believe that the numerical results presented in this work provide tests and motivations for such theories.

Acknowledgments

M. S. was supported by the National Science Foundation and A. D. and S. T. were partially supported by the National Science Foundation under Grant No. DMS-0312067.

- [1] S. Torquato, T. M. Truskett, and P. G. Debenedetti, *Phys. Rev. Lett.* **84**, 2064 (2000).
- [2] A. R. Kansal, S. Torquato, and F. H. Stillinger, *Phys. Rev. E* **66**, 041109 (2002).
- [3] A. Donev, S. Torquato, and F. H. Stillinger, *Phys. Rev. E* **71**, 011105 (2005).
- [4] A. Donev, F. H. Stillinger, and S. Torquato, *Phys. Rev. Lett.* **95**, 090604 (2005).
- [5] M. D. Rintoul and S. Torquato, *Phys. Rev. Lett.* **77**, 4198 (1996).
- [6] A. Donev, F. H. Stillinger, and S. Torquato, *Phys. Rev. Lett.* **96**, 225502 (2006).
- [7] J. L. Finney, *Proc. R. Soc. Lond. A* **319**, 479 (1970).
- [8] C. H. Bennett, *J. Appl. Phys.* **32**, 2727 (1972).
- [9] J. Tobochnik and P. M. Chapin, *J. Chem. Phys.* **88**, 5824 (1988).
- [10] A. Z. Zinchenko, *J. Comput. Phys.* **114**, 298 (1994).
- [11] N. Xu, J. Blawdziewicz, and C. O'Hern, *Phys. Rev. E* **71**, 061306 (2005).
- [12] P. M. Chaikin and T. C. Lubensky, *Principles of condensed matter physics* (Cambridge University Press, Cambridge, United Kingdom, 1995).
- [13] M. Luban and A. Baram, *J. Chem. Phys.* **76**, 3233 (1982).
- [14] C. J. Joslin, *J. Chem. Phys.* **77**, 2701 (1982).
- [15] M. Luban and J. P. J. Michels, *Phys. Rev. A* **41**, 6796 (1990).
- [16] M. Bishop, A. Masters, and J. H. R. Clarke, *J. Chem. Phys.* **110**, 11449 (1999); M. Bishop, A. Masters, and A. Y. Vlasov, *J. Chem. Phys.* **121**, 6884 (2004); M. Bishop, A. Masters and A. Yu. Vlasov, *J. Chem. Phys.* **122**, 154502 (2005); M. Bishop and P.A. Whitlock, *J. Chem. Phys.* **123**, 014507 (2005).
- [17] N. Clisby and B. McCoy, *J. Stat. Phys.* **114**, 1343 (2004); *ibid.*, 1361 (2004); *ibid.*, **122**, 15 (2006); N. Clisby and B.M. McCoy, *J. Phys.* **64**, 775 (2005).
- [18] I. Lyberg, *J. Stat. Phys.* **119**, 747 (2005).
- [19] N. Clisby and B. McCoy, *J. Stat. Phys.* **122**, 15 (2006).
- [20] H. L. Frisch and J. K. Percus, *Phys. Rev. E* **60**, 2942 (1999).

- [21] G. Parisi and F. Slanina, *Phys. Rev. E* **62**, 6554 (2000).
- [22] R. Finken, M. Schmidt, and H. Lowen, *Phys. Rev. E* **65**, 016108 (2001).
- [23] S. Torquato, *Random Heterogeneous Materials: Microstructure and Macroscopic Properties* (Springer-Verlag, New York, 2002).
- [24] A. P. Philipse, *Colloids and Surfaces A* **213**, 167 (2003).
- [25] S. Torquato and F. H. Stillinger, *Phys. Rev. E* **68**, 041113 (2003).
- [26] G. Parisi and F. Zamponi, *J. Stat. Mech.* p. P03017 (2006).
- [27] S. Torquato and F. H. Stillinger, *Experimental Math.* (in press).
- [28] S. Torquato and F. H. Stillinger, *Phys. Rev. E* **73**, 031106 (2006).
- [29] S. Torquato, O. U. Uche and F. H. Stillinger, in preparation.
- [30] J. H. Conway and N. J. A. Sloane, *Sphere Packings, Lattices, and Groups* (Springer-Verlag, New York, 1998).
- [31] L. Lue, *J. Chem. Phys.* **122**, 044513 (2005).
- [32] M. Bishop, P. Whitlock, and D. Klein, *J. Chem. Phys.* **122**, 074508 (2005).
- [33] J. P. J. Michels and N. J. Trappaniers, *Phys. Lett. A* **104**, 425 (1984).
- [34] T. C. Hales, *Ann. Math.* **162**, 1065 (2005), see also T. C. Hales, arXiv:math.MG/9811078 (1998).
- [35] O. Musin, technical Report, Moscow State University, 2004.
- [36] G. D. Scott and D. M. Kilgour, *Brit. J. Appl. Phys.* **2** 863 (1969).
- [37] S. Torquato and F. H. Stillinger, *J. Phys. Chem. B* **105**, 11849 (2001).
- [38] S. Torquato, A. Donev, and F. H. Stillinger, *Int. J. Solids Structures* **40**, 7143 (2003).
- [39] A. Donev, S. Torquato, F. H. Stillinger, and R. Connelly, *J. Comp. Phys.* **197**, 139 (2004).
- [40] Ref. [28] presents the first exactly solvable disordered sphere-packing model (“ghost random sequential addition packing) in arbitrary space dimension. Specifically, it was shown that all of the n -particle correlation functions of this nonequilibrium model can be obtained analytically for all allowable densities and in any dimension. It provides an exact demonstration of the decorrelation principle; see also Ref. [27]
- [41] B. D. Lubachevsky and F. H. Stillinger, *J. Stat. Phys.* **60**, 561 (1990).
- [42] A. Donev, S. Torquato, and F. H. Stillinger, *J. Comp. Phys.* **202**, 737 (2005).
- [43] M. Ross and B. J. Alder, *Phys. Rev. Lett.* **16**, 1077 (1966).
- [44] W. B. Streett, H. J. Raveche, and R. D. Mountain, *J. Chem. Phys.* **61**, 1960 (1974).

- [45] D. Frenkel and B. Smit, *Understanding Molecular Simulation* (Academic Press, 2002).
- [46] Z. W. Salsburg and W. W. Wood, *J. Chem. Phys.* **37**, 798 (1962).
- [47] R. J. Speedy, *J. Phys. Condens. Matter* **10**, 4387 (1998).
- [48] P. M. Chaikin, *Soft and Fragile Matter, Nonequilibrium Dynamics, Metastability and Flow* (*M. E. Cates and M. R. Evans, editors*) (Institute of Physics Publishing, London, 2000), chap. Thermodynamics and Hydrodynamics of Hard Spheres; the role of gravity, pp. 315–348.
- [49] The specific extrapolation function we use for both $d = 4$ and $d = 5$ is of the form

$$\Delta Z(x) = a_1 x e^{-a_2 x} \cos(a_3 x + a_4),$$

where a_1, a_2, a_3 , and a_4 are fitting parameters.

- [50] A saturated packing is one that contains no voids large enough to accommodate an additional particle; see Ref. 20, for example.
- [51] Due to computational constraints, our packings for $d = 6$ were produced with a relatively high expansion rate ($\gamma = 10^{-3}$) and were not grown to sufficiently high pressures, as necessary to properly distinguish between true contacts and near contacts; therefore, we do not show results for $d = 6$ in this section.